This is the accepted manuscript made available via CHORUS. The article has been published as:

Bond-Selected Photodissociation of Single Molecules Adsorbed on Metal Surfaces

Shaowei Li (□□□), Gregory Czap, Hui Wang, Likun Wang, Siyu Chen (□□□), Arthur Yu, Ruqian Wu, and W. Ho

Phys. Rev. Lett. **122**, 077401 — Published 22 February 2019

DOI: 10.1103/PhysRevLett.122.077401

Bond-selected Photodissociation of Single Molecules Adsorbed on Metal Surfaces

Shaowei Li（李绍巍）,[†] Gregory Czap,[†] Hui Wang,[†] Likun Wang,[†] Siyu Chen (陈思宇),[†]

Arthur Yu,[†] Ruqian Wu,[†,*] and W. Ho[†,‡,*]

[†]Department of Physics and Astronomy, University of California, Irvine, CA 92697-4575

[‡]Department of Chemistry, University of California, Irvine, CA 92697-2025

We report the photo-assisted activation of selected C-H bonds in individual molecules adsorbed on metal surfaces within the junction of a scanning tunneling microscope. Photons can couple to the C-H bond activation of specific hydrocarbons through a resonant photo-assisted tunneling process. The molecule to be activated can be selected by positioning the tip with sub-Ångström resolution. Furthermore, structural tomography of the molecule and its dissociation products are imaged at different heights by the inelastic tunneling probe. The demonstration of single bond dissociation induced by resonant photo-assisted tunneling electrons implies the attainment of atomic scale spatial resolution for bond-selected photochemistry.

The desire for increasingly finer details in optical microscopy, particularly in revealing the fundamental properties of molecules and low dimensional materials, has driven rigorous development in imaging techniques far beyond the diffraction limit. The ability to reach atomic scale resolution would ultimately provide an optical probe with the highest spatial resolution to date. It is well established that the scanning tunneling microscope (STM) provides a wealth of information on low dimensional molecular systems. The STM has been shown to be an ideal tool to induce and detect surface reactions with sub-molecular precision [1], to break and form individual bonds [2,3]. Experiments with the STM have significantly enriched our understanding of the material composition [4,5], molecular organization [6,7], intra- and inter-molecular coupling [8,9], and molecular structure [10]. Furthermore, the coupling of photon excitation with electron tunneling in the STM junction unites the advantages of optical measurements with the Ångström resolution of tunneling electrons, enabling the studies of photo-induced chemical processes such as single electron transfer [11,12] and nuclear motions of single molecules [13-15] at the atomic scale.

The controlled activation of inert carbon-hydrogen (C-H) bonds in hydrocarbons has been a ubiquitous theme in organic chemistry [16-19]. Photo-induced C-H scissions are especially appealing since they utilize the energy of light to activate thermodynamically unfavorable reactions [20]. However, a common difficulty with all previous studies involves the selective activation of a designated C-H bond [21], especially if there are multiple equivalent bonds within one molecule.

In this study, we investigated the coupling of photons to activate the C-H bonds of azulene adsorbed on Ag(110), and additionally acetylene (HCCH) and ethynyl radical (CCH) adsorbed on Cu(001) in the STM junction. We demonstrate the selective dissociation of a single

C-H bond in a single molecule by coupling photons from a Ti-sapphire laser to the tunneling process. A tunneling electron can gain energy from a laser photon to induce the scission of a single chemical bond. The reaction can be visualized by the distinct change of the molecule in constant current topography and high-resolution inelastic tunneling probe (itProbe) images [10]. We can precisely control the desired reaction product by shifting the tip position over the molecule with sub-Ångström spatial resolution.

The azulene molecule is an organic dye and is widely studied in photochemical processes. Individual azulene molecules appear as a pear shape on the Ag(110) surface as shown in Fig. 1(a). and Fig. 1(g). The molecules adsorb in two equivalent geometries [image shown in Fig. 1(g) and its equivalent rotated by 180°] with their long axis along the [001] direction of the substrate. A low coverage of CO molecules [round depressions in Fig. 1(f)] are co-adsorbed on the surface to allow more detailed structural determination with a CO terminated tip.

In the absence of laser illumination, the azulene molecules can be consistently converted to different species when the bias is set higher than 2.4 V. The type of converted species can be controlled by positioning the STM tip, as shown in Fig. S1 in the Supplemental Material [22]. When the tip is located at the position marked in Fig. S1(g), designated conversion to a crescent-shaped product can occur [Fig. 1(a)-(e), (h)]. The dependence of the tip-height z vs. bias recorded over the molecule shows a stepwise change associated with the bond dissociation as the bias ramps from low to high with the feedback on (Fig. S2). If the bias is ramped again over the opposite edge of the “crescent” product, the molecule can be further changed to a peanut-shaped product [Fig. 1(e), (i)], which is relatively stable and difficult to undergo further conversion. The conversion process is highly localized. A series of topographic images taken over three nearby

azulene molecules irradiated by light is shown in Fig. 1(a)-(e). Each individual molecule can be converted to the desired products without affecting other nearby molecules.

Each irreversible change in the molecular topography indicates that the molecule has undergone a chemical transformation. The semi-constant height itProbe images resolve the skeletal structures of the azulene molecule and its products. The image of an intact azulene molecule shows clearly a seven-membered ring attached to a five-membered ring and the relatively dimmer C-H features [Fig. 1(j)]. Density functional theory (DFT) calculations have reproduced the adsorption geometries of azulene on Ag(110) [Fig. 1(m)] and the two products [Fig. 1(n),(o)]. Compared to the intact molecule whose long molecular axis is along the [001] direction, the "crescent" product shown in Fig. 1(n) is rotated by 30 degrees clockwise. A relatively brighter line in the itProbe image of Fig. 1(k) is resolved near the position where the tip was parked to induce the reaction. This new feature indicates the formation of a chemical bond between the carbon atom of the seven-membered ring and a substrate Ag atom after the dissociation of the C-H bond. The molecule tilts upward and contributes to the asymmetric topographic image in Fig. 1(h) and the distorted ring features in the semi-constant height itProbe image in Fig. 1(k). The "peanut" product is further rotated by another 30 degrees clockwise compared to the "crescent". Two relatively brighter lines correspond to the two C-Ag bonds that are resolved by the itProbe on both sides of the seven-membered ring where the sequential scissions of two C-H bonds have occurred. The molecule is adsorbed in a boat structure with both ends tilted upward along the molecular axis [Fig. 2(i)].

The non-planar molecular adsorption geometries can be better resolved by acquiring constant-height itProbe images at different tip heights. Similar to non-contact atomic force microscopy [23-25], the imaging contrast of atoms and bonds in itProbe arises from short range

repulsive forces. Images by itProbe are therefore sensitive to the heights of atoms in non-planar molecules, with the most protruding atoms being imaged at the largest tip-substrate distances and atoms closer to the surface requiring smaller tip-substrate distances to resolve. The intact molecule shows an overall planar geometry in the images taken with three different tip-substrate separations as shown in Fig. 2(a), 2(d), and 2(g). The five-membered and seven-membered carbon rings are resolved when the tip is relatively far away [Fig. 2(a)]. The features corresponding to C-H bonds start to appear when the tip gets close to the molecule [Fig. 2(g)]. For the "crescent" product, the corner edge of the seven-membered ring can be resolved at the largest tip-substrate distance in Fig. 2(b), corresponding with the highest part of the molecule that is consistent with the adsorption geometry given by the DFT calculation. One side of the molecule has a significantly higher contrast (brighter) than the other side in Fig. 2(h), further confirming the side-tilted geometry as shown in Fig. 2(k). For the "peanut' product shown in Fig. 2(c), 2(f), and 2(i), the two ends of the molecule are resolved at a higher height than the middle section, again matching the calculated geometry shown in Fig. 2(l). The good agreement between the itProbe images and the DFT calculations confirms the identities and structures of azulene and the two dissociation products.

Without laser illumination, the C-H bond of an intact azulene molecule cannot be activated when the bias is below 2.4 V. However, with the junction illuminated, the localized dissociation of the molecule occurs at a much lower threshold bias. The molecule shown in Fig. 1(a) was dissociated into the "crescent" product with only 1.2 V bias. The "crescent" molecule in Fig. 1(d) was further converted to a "peanut" in Fig. 1(e) with the bias set at 0.6 V.

To quantify the photon-induced chemical transformation, we have compared the C-H bond dissociation rates at different sample bias in the dark and with laser illumination. Methods

of the dissociation rate measurement are described in the Supplemental Material [22]. The dependence of the dissociation rate on the sample bias shows a clear threshold with laser irradiation or in the dark. Reactions could be observed at a bias as low as 0.9 V when the junction was irradiated with 820 nm light as laser pulses [Fig. 3(a)-(b)] or in the continuous wave (CW) mode (Fig. S7), compared to the threshold bias of 2.4 V in the dark. The energy difference (1.5 eV) between these two thresholds matches the photon energy of the 820 nm laser light, indicating the quantum-mechanical coupling of the photons to the tunneling electrons. The reaction rate increases exponentially with bias voltage. A qualitative discussion of the exponential behavior for the dissociation rate vs. bias voltage is presented in the Supplemental Material [22].

We have also investigated the photo-assisted scission of HCCH and CCH on Cu(001). Interestingly, we found that the laser induced dissociation discriminates different molecules. Similar to azulene, the minimum bias required to dissociate a CCH into a dicarbon (CC) is reduced from 2.2 V to 0.7 V under laser illumination. However, no laser induced C-H bond dissociation was observed for HCCH to CCH. Detailed discussions of the C-H activation in acetylene and ethynyl can be found in the Supplementary Material [22].

The photoexcitation of a molecule in the STM junction involves the coupling of photon with both junction plasmon and tip-molecule-substrate electronic states. The three possible excitation pathways are illustrated in Fig. 3(c-e). In the first pathway [Fig. 3(c)], an electron in the STM tip is excited to a state with *hv* energy higher than the Fermi level by absorbing a photon, following by tunneling to the molecule to induce a reaction. This mechanism was previously used to explain the photo-assisted tunneling in semiconductor junctions [26,27]. However, this non-resonant photo-assisted tunneling model is not molecule-specific and cannot

account for the absence of photo-effect in the dissociation of acetylene. The selective coupling of a photon to certain molecules indicates the importance of molecular properties, such as molecular orbitals, in the photon-electron coupling process. The second pathway involves photoexcitation of the molecule-substrate, followed by an Auger-like process leading to an excited electron [Fig. 3(d)]. However, this pathway should be independent of the direction of tunneling current. The absence of photo-dissociation at negative bias excludes this pathway from the dominate mechanism for the photodissociation. The third pathway is illustrated by the resonant photo-assisted tunneling mechanism in Fig. 3(e). the photon excites a tunneling electron occupying an initial state that is composed of a molecular orbital hybridized with the substrate band structure. This resonant photo-assisted tunneling model was previously used to explain the photo-assisted transport in nano-structures or quantum dots [28,29]. Compared to the first pathway, the cross section for photo-excitation of the electrons in the STM tip is expected to be larger than for the electron in a single molecule in the junction due to the larger physical size of the tip. However, the coupling of light to the localized junction plasmon could strongly enhance the cross section of the resonant photo-assisted tunneling [22,30].

The cross section of the resonant photo-assisted tunneling pathway depends on the molecular density of state that is in resonance with the initial state for the photo-assisted tunneling electron. Confidence in this mechanism can be gained from measuring the electronic structure of azulene on Ag(110) with scanning tunneling spectroscopy (STS) and by DFT calculations. A broad electronic peak corresponding to azulene's lowest unoccupied molecular orbital (LUMO) spans from 0.3 V to 1 V and centers around 0.5 V in the *dI/dV* spectra obtained at the center of an azulene molecule. Results from DFT calculations show the LUMO at 0.5 eV above the Fermi level with a density of states spanning from 0.3 eV to 1 eV. The *dI/dV* image

[inset of Fig. 4(a)] shows a four-lobed structure that closely resembles the spatial distribution of LUMO given by DFT [Fig. 4(b)] [30,31]. The role of resonant photo-assisted tunneling is further validated by the absence of electronic states for acetylene that is in resonance with the tunneling electron. DFT calculations indicate that both azulene and ethynyl have molecular orbitals spanning from 0.5 eV to 2.0 eV above the Fermi level whereas the acetylene molecule has a very low density of states in this energy range [Fig. 4(b) and Fig. S6]. Therefore, the cross section of the resonant photo-assisted tunneling pathway for acetylene is much smaller than azulene and ethynyl. [32,33]. On the other hand, the two pathways in Fig. 3(c) and 3(d) could also contribute to the C-H photodissociation. Additional theoretical and experimental work is necessary to thoroughly understand the mechanism of the observed atomic scale localization of photo-dissociation.

The activation barrier for converting an azulene to a "crescent" product is found to be 2.6 eV by DFT calculations as shown in Fig. 4(c), in close agreement with the measured reaction threshold of 2.4 eV in the absence of laser illumination. The calculated structures of the azulene and its intermediates during the dissociation of the first C-H bond [Fig. 4(d)] and the second C-H bond [Fig. 4(e)] show the ejection of the hydrogen and the subsequent structural changes in the two products.

We have demonstrated the selective activation of a single molecule assisted by laser photons. The realization of the coupling of laser photons and tunneling electrons in the STM junction enables the study of photochemistry with submolecular resolution. The ability to combine localized laser field in the STM junction with electron tunneling allows the selected photo-activation of individual chemical bonds in a single molecule. Our study provides a new approach to induce and visualize photochemical processes in real space.

This work was supported by the National Science Foundation Center for Chemical Innovation on Chemistry at the Space-Time Limit (CaSTL) under Grant No. CHE-1414466.

*To whom all correspondence should be addressed.
wilsonho@uci.edu, wur@uci.edu

References

[1] W. Ho, Acc. Chem. Res. **31**, 567 (1998).

[2] H. J. Lee and W. Ho, Science **286**, 1719 (1999).

[3] Y. Jiang, Q. Huan, L. Fabris, G. C. Bazan, and W. Ho, Nat. Chem. **5**, 36 (2013).

[4] C. Weiss, C. Wagner, C. Kleimann, M. Rohlfing, F. S. Tautz, and R. Temirov, Phys. Rev. Lett. **105**, 086103 (2010).

[5] L. Gross, N. Moll, F. Mohn, A. Curioni, G. Meyer, F. Hanke, and M. Persson, Phys. Rev. Lett. **107**, 086101 (2011).

[6] Z. Han, G. Czap, C. Xu, C. L. Chiang, D. Yuan, R. Wu, and W. Ho, Phys. Rev. Lett. **118**, 036801 (2017).

[7] S. Li, D. Yuan, A. Yu, G. Czap, R. Wu, and W. Ho, Phys. Rev. Lett. **114**, 206101 (2015).

[8] G. V. Nazin, X. H. Qiu, and W. Ho, Science **302**, 77 (2003).

[9] C. Weiss, C. Wagner, R. Temirov, and F. S. Tautz, J. Am. Chem. Soc. **132**, 11864 (2010).

[10] C. L. Chiang, C. Xu, Z. Han, and W. Ho, Science **334**, 885 (2014).

[11] S. W. Wu, N. Ogawa, and W. Ho, Science **312**, 1362 (2006).

[12] S. W. Wu and W. Ho, Phys. Rev. B **82**, 085444 (2010).

[13] T. L. Cocker, D. Peller, P. Yu, J. Repp, and R. Huber, Nature **539**, 263 (2016).

[14] L. Bartels, F. Wang, D. Moeller, E. Knoesel, and T. Heinz, Science **305**, 648 (2004).

[15] S. Li, S. Chen, J. Li, R. Wu, and W. Ho, Phys. Rev. Lett. **119**, 176002 (2017).

[16] T. W. Lyons and M. S. Sanford, Chem. Rev. **110**, 1147 (2010).

[17] L. McMurray, F. O'Haraa, and M. Gaunt, J. Chem. Soc. Rev. **40**, 1885 (2011).

[18] B. S. Greensfelder, H. H. Voge, and G. M. Good, Ind. Eng. Chem. **41**, 2573 (1949).

[19] J. A. Labinger and J. E. Bercaw, Nature **417**, 507 (2002).

[20] N. A. Romero and D. A. Nicewicz, Chem. Rev. **116**, 10075 (2016).

[21] Z. Zhang, K. Tanaka, and J. Q. Yu, Nature **543**, 538 (2017).

[22] See Supplemental Material at http://link.aps.org/supplemental/xxx for details of experiment and DFT methods, supplemental figures, and Refs. [10, 34-45].

[23] N. Pavliček, B. Fleury, M. Neu, J. Niedenführ, C. Herranz-Lancho, M. Ruben, and Jascha Repp, Phys. Rev. Lett. **108**, 086101 (2012).

[24] B. Schuler, W. Liu, A. Tkatchenko, N. Moll, G. Meyer, A. Mistry, D. Fox, and Leo Gross Phys. Rev. Lett. **111**, 106103 (2013).

[25] B. Schuler, S. Fatayer, F. Mohn, N. Moll, N. Pavliček, G. Meyer, D. Peña, and L. Gross Nature Chem. **8**, 220 (2016).

[26] S. P. Apell and D. R. Penn, Phys. Rev. B **45**, 6757 (1992).

[27] A. Thon, M. Merschdorf, W. Pfeiffer, T. Klamroth, P. Saalfrank, and D. Diesing, Appl. Phys. A **78**, 189 (2004).

[28] G. Platero and R. Aguado, Phys. Rep. **395**, 1 (2004).

[29] K. Shibata, A. Umeno, K. M. Cha, and K. Hirakawa, Phys. Rev. Lett. 109, 077401 (2012).

[30] A. Yu, S. Li, H. Wang, S. Chen, R. Wu, and W. Ho, Nano. Lett. **18**, 3076 (2018).

[31] S. Chiang, Chem. Rev. **97**, 1083 (1997).

[32] W. Ho, J. Phys. Chem. **100**, 13050 (1996).

[33] F.M. Zimmermann and W. Ho, Surf. Sci. Rep. **22**, 127 (1995).

[34] B. C. Stipe, M. A. Rezaei, and W. Ho, Rev. Sci. Instrum. **70**, 137 (1999).

[35] G. Kresse and J. Hafner, Phys. Rev. B **49**, 14251 (1994).

[36] G. Kresse and D. Joubert, Phys. Rev. B **59**, 1758 (1999).

[37] P. E. Blochl, Phys. Rev. B **50**, 17953 (1994).

[38] J. P. Perdew, K. Burke, and M. Ernzerhof, Phys. Rev. Lett. **77**, 3865 (1996).

[39] S. Grimme, J. Antony, S. Ehrlich, and S. Krieg, J. Chem. Phys. **132**, 154104 (2010).

[40] S. Li, A. Yu, F. Toledo, Z. Han, H. Wang, H. Y. He, R. Wu, and W. Ho, Phys. Rev. Lett. **111**, 146102 (2013).

[41] H. Wang, S. Li, H. Y. He, A. Yu, F. Toledo, Z. Han, W. Ho, and R. Wu, J. Phys. Chem. Lett. **6**, 3453 (2015).

[42] H. J. Monkhorst and J. D. Pack, Phys. Rev. B **13**, 5188 (1976).

[43] L.J. Lauhon and W. Ho, Phys Rev. Lett. **84**, 1527 (2000).

[44] E. Kazuma, J. Jung, H. Ueba, M. Trenary, and Yousoo Kim, Science **360**, 521 (2018).

[45] E. Kazuma, J. Jung, H. Ueba, M. Trenary, and Yousoo Kim, J. Am. Chem. Soc. **139**, 3115 (2017).

FIGURE CAPTIONS

FIG. 1. (a-e) A series of STM topographic images taken before and after dissociating several nearby azulene molecules with laser illumination. The arrows indicate the positions over which the tip was parked. The molecules can be turned into a "crescent" shape as shown in (b-d). A "crescent" species indicated by the arrow in (d) further dissociated into a "peanut" shape as shown in (e). (f) Topographic image showing an intact azulene molecule and two dissociation products. The round depressions are the co-adsorbed CO molecules. (g-i) Zoom-in STM topographic images of the intact azulene molecule (g), the "crescent" product (h), and the "peanut" product (i). (a-e) were taken with 0.5 V and 1 nA set points in constant current mode. (j-l) The semi-constant height itProbe images of azulene and the two products corresponding to the molecules shown in (g-i). (m-o) Top views of the adsorption structures given by DFT calculations of the intact azulene (m), after one C-H bond scission (n), and after scission of two C-H bonds (o).

FIG. 2. (a-c) Constant height itProbe images of (a) an intact azulene, (b) a "crescent" product, and (c) a "peanut" product, taken with feedback off at 100 mV, 0.1 nA and over the center of the molecule, followed by advancing the tip 0.59 Å towards the molecule. (d-i) The constant height itProbe images taken with the tip advanced 0.72 Å (d-f) and 0.85 Å (g-i) towards the molecule. (j-l) Side views of the adsorption structures given by DFT calculations of azulene and its dissociation products.

FIG. 3. (a) The azulene dissociation rate as a function of bias with (red) or without (black) pulse laser illumination. The red and black lines are the exponential fits to the data. (b) The semi-log

plot of the data in (a). (c-e) Schematic diagrams of three possible mechanisms of electron-photon coupling in the STM junction.

FIG. 4. (a) *dI/dV* spectra taken over the center of an azulene molecule (red) and Ag(110) background (black). The inset shows the *dI/dV* image taken at 0.9 V. (b) Calculated density of states of an azulene adsorbed on Ag (110). The HOMO is found at 1.6 eV below the Fermi level. The LUMO and LUMO+1 are found at 0.5 eV and 1.3 eV above the Fermi level, respectively. The insets show the spatial distributions of the local density of states of HOMO, LUMO, and LUMO+1. Red indicates occupied states and blue indicates the empty states. (c) DFT calculations of the activation barriers of dissociating an azulene into a "crescent" product (black) and dissociating a "crescent" product into a "peanut" product (red). To determine the energies of the transition states, we stretch out the C to H distance in the DFT model and allow the molecule to relax to a locally optimized structure. The open symbols denote the C to H distance before relaxation and the solid symbols after relaxation. (d,e) Top views (top) and side views (bottom) of the calculated intermediate structures of the molecule during the first (d) and second (e) C-H bond dissociation. The corresponding energies and positions along the C to H reaction coordinate are labeled in (c).

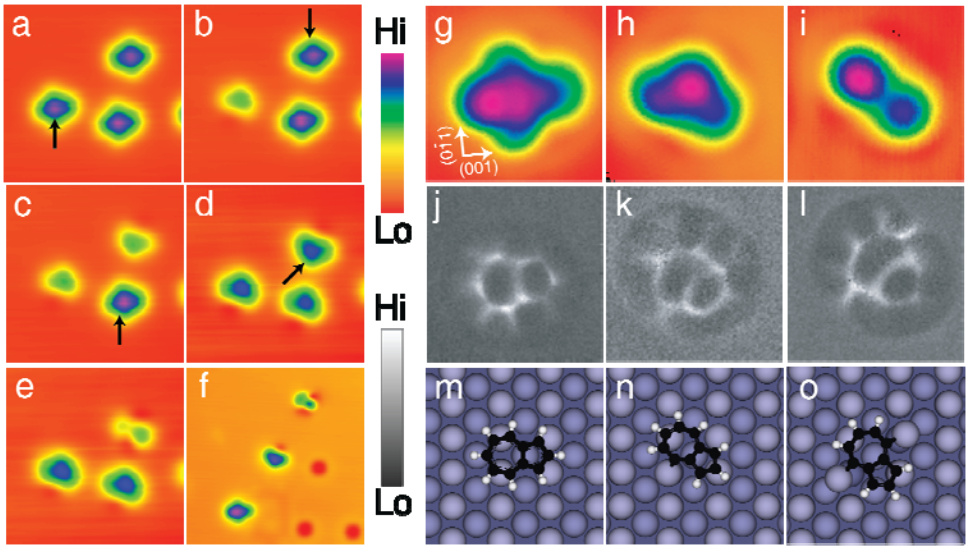

FIG. 1.

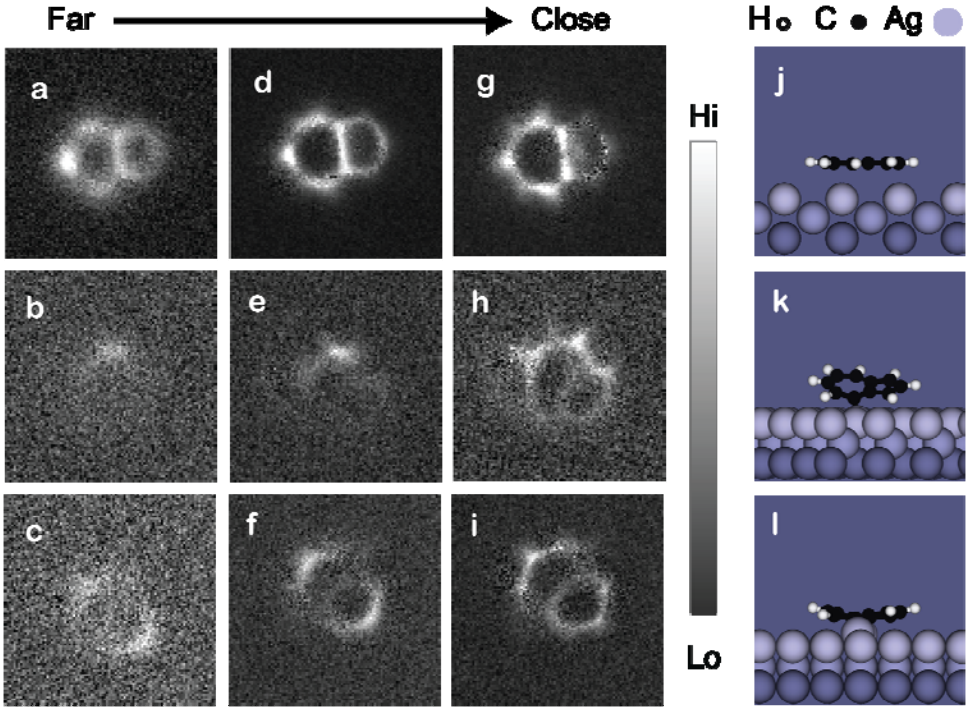

FIG. 2.

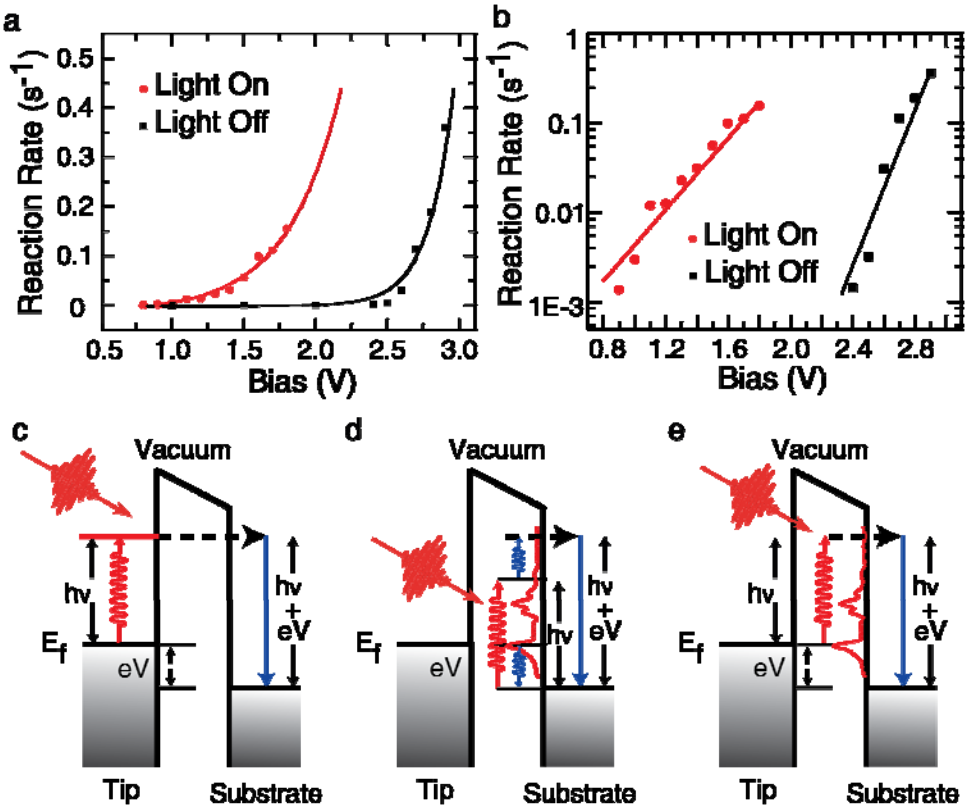
a
Reaction Rate (s-1)
Light On
Light Off
Bias (V)
b
Reaction Rate (s-1)
Light On
Light Off
Bias (V)
c
Vacuum
hv
Ef
eV
hv + eV
Tip
Substrate
d
Vacuum
hv
Ef
eV
hv + eV
Tip
Substrate
e
Vacuum
hv
Ef
eV
hv + eV
Tip
Substrate

FIG. 3.

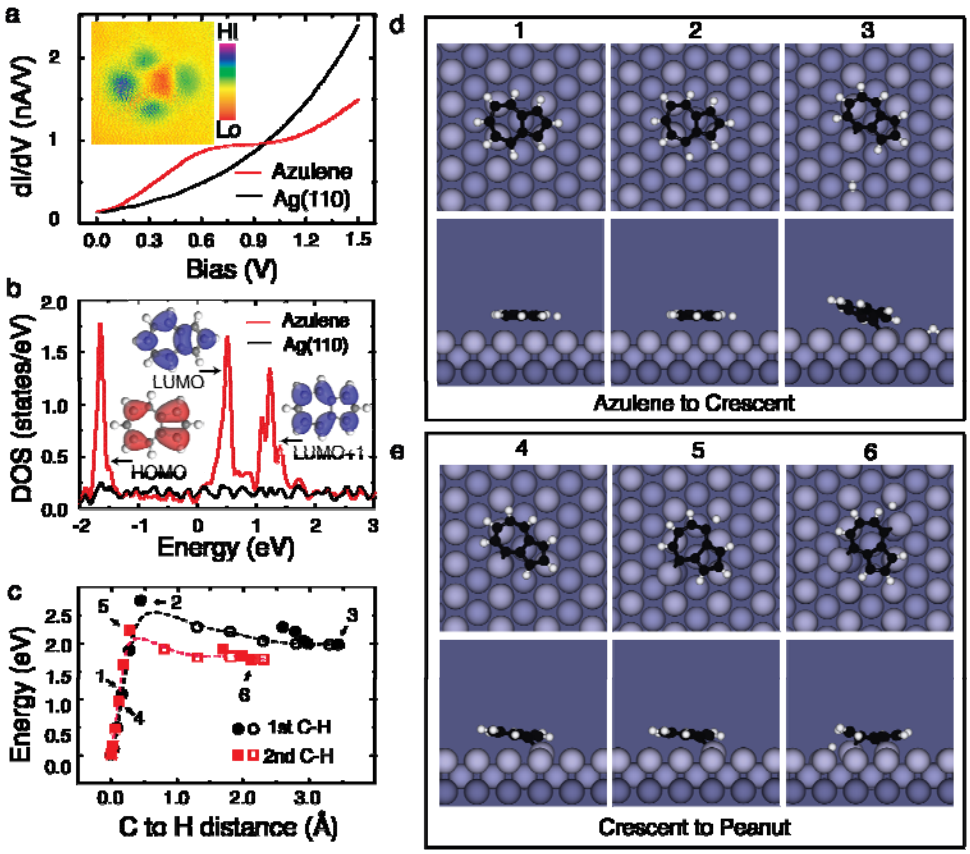
a
dI/dV (nA/V)
Hi
Lo
Azulene
Ag(110)
Bias (V)
b
DOS (states/eV)
Azulene
Ag(110)
LUMO
HOMO
LUMO+1
Energy (eV)
c
Energy (eV)
1st C-H
2nd C-H
C to H distance (Å)
d
1
2
3
Azulene to Crescent
e
4
5
6
Crescent to Peanut

FIG. 4.